Patient no.	Age (years)	Gender	Affected eye						Fellow eye					
			78.20 cd/m²	31.87 cd/m²	11.37 cd/m²	4.14 cd/m²	1.30 cd/m²	0.37 cd/m²	78.20 cd/m²	31.87 cd/m²	11.37 cd/m²	4.14 cd/m²	1.30 cd/m²	0.37 cd/m²
1	39	M	0.01	0.12	0.15	0.27	0.55	N.R.	-0.04	0	0	0.03	0.13	0.35
2	41	F	0.16	0.16	0.24	0.3	0.46	0.64	0.03	0.06	0.12	0.17	0.34	0.45
3	50	F	0.16	0.28	0.31	0.5	0.65	N.R.	0.1	0.22	0.31	0.4	0.42	0.55
4	41	M	0.13	0.29	0.3	0.41	0.58	0.76	0.03	0.02	0.07	0.17	0.18	0.45
5	40	M	0.17	0.32	0.39	0.52	0.72	N.R.	0.06	0.06	0.1	0.22	0.31	0.49
6	39	M	0.15	0.23	0.26	0.37	0.59	N.R.	0.04	0.07	0.1	0.24	0.35	0.5
7	39	M	0.1	0.22	0.36	0.6	0.76	N.R.	0.01	0	0.1	0.2	0.29	0.36

Visual acuities are shown as logMAR. M = male, F = female, N.R. = not recordable

Table 1. Visual acuities under different background luminances in patients with central serous chorioretinopaty.

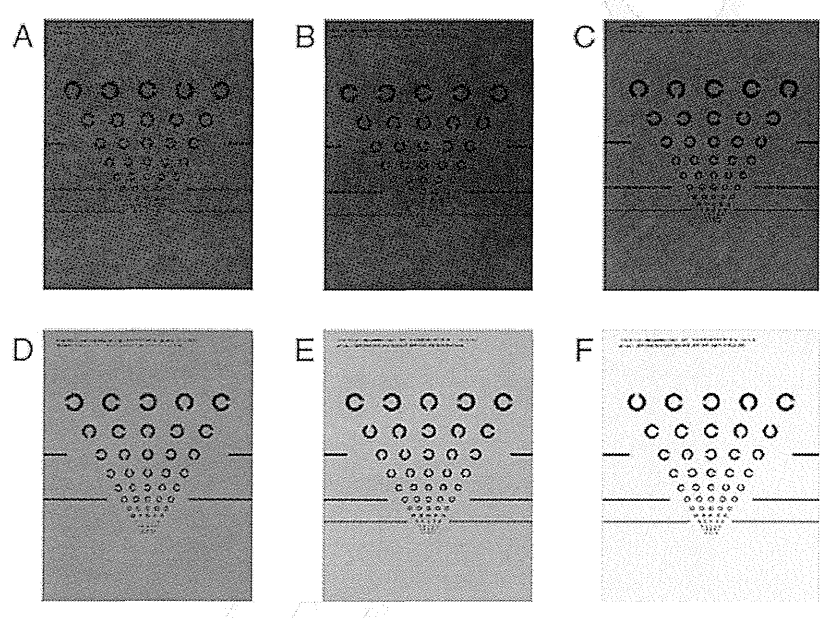

Figure 2. Low luminance visual acuity charts. The background luminance values were (A) 0.37 cd/m², (B) 1.30 cd/m², (C) 4.14 cd/m², (D) 11.37 cd/m², (E) 31.87 cd/m² and (F) 78.20 cd/m².

Case	Age	Gender	OCT parameter (μm)			Low luminance visual acuity			
			FT	SRDH	SRDW	a	b	R^2	p
1	39	M	183.3	275.0	2703.1	-0.121	0.5098	0.9079	0.0122
2	41	F	216.7	141.7	1171.9	-0.091	0.4932	0.9292	0.0193
3	50	F	244.1	141.1	2458.2	-0.118	0.6607	0.9636	0.0030
4	41	M	180.7	231.4	3004.7	-0.111	0.6143	0.9648	0.0005
5	40	M	191.7	308.3	2745.0	-0.127	0.7278	0.9811	0.0011
6	39	M	183.1	404.3	4086.0	-0.101	0.5603	0.9171	0.0104
7	39	M	181.2	322.1	3239.9	-0.166	0.8049	0.9894	0.0005

M = male, F = female, OCT = optical coherence tomography, these parameters are indicated in Figure 1.
FT = foveal thickness, SRDH = height of the serous retinal detachment, SRDW = width of serous retinal detachment. When low luminance visual acuity was plotted against background luminance as shown in Figure 1, the following formula was fitted: $y = a * X + b$, when y indicates log MAR and x indicates log (luminance), R^2: coefficient of regression

Table 2. Parameters of the optical coherence tomographic image and fitting of low luminance visual acuity in eyes with central serous chorioretinopathy

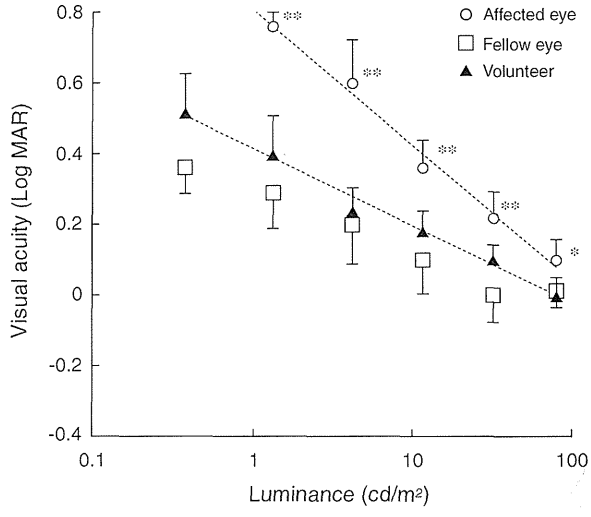

Figure 3. Relationship between logMAR visual acuity (VA) and the log background luminance. The data were fitted by the least square method and a linear equation between the logMAR VA and log luminance for the three groups. The logMAR VA is linearly correlated with the luminance. The logMAR VA of the eye with central serous chorioretinopathy is significantly higher than that of the fellow eye at each luminance level. Visual acuities at all levels of luminance except 0.37cd/m^2 are significantly different between central serous chorioretinopathy and the eyes of normal volunteers (*$p < 0.05$, **$p < 0.01$). ○: affected eye, □: fellow eye, △: normal eye of control participants, Error bars indicate standard deviation.

Thus, we developed a computer program which allowed us to create Landolt Cs on a computer monitor screen with different background luminances. With these targets and background luminances, we were able to evaluate how luminance levels affected the VA in central serous chorioretinopathy patients.

Shlaer[4] reported that lower background luminances led to lower VA in normal eyes and we obtained similar results in our normal eyes. The VA of eyes with central serous chorioretinopathy also decreased according to the decrease in background luminance but the deterioration was more severe than that of normal eyes at all background luminance levels. We found that VA in logMAR units was linearly correlated with the logarithm of the background luminance. The logMAR VA in eyes with central serous chorioretinopathy was significantly higher, that is, poorer VA, than that in normal control eyes.

Hypotheses have been presented to explain the decreased VA under low luminance in normal eyes.[13,14] Thus, Hecht[13] suggested that the number of cone photoreceptors activated is decreased at low luminances. Our subjects were dark-adapted for seven minutes before testing and the cone system was expected to be functioning during this period in a healthy retina, and all of the normal fellow eyes could see at the lowest background luminance. Five of seven eyes with central serous chorioretinopathy could not identify even one Landolt C at the lowest luminance level, although the VA measured under standard conditions was at least 0 logMAR units in all eyes. These findings suggest that the foveal cones are not functioning normally in low light conditions in eyes with central serous chorioretinopathy.

Chuang and colleagues[15] reported that the rods were more affected than cones in eyes with central serous chorioretinopathy; however, they did not evaluate the rods selectively to determine whether the cones were indeed normal. The decreased VA measured under mesopic conditions in our study is probably due to impairments of both cone and rod function. This is consistent with the results of the Humphrey perimetric retinal sensitivity decrease in the detached area in eyes with central serous chorioretinopathy.[9]

Recent advances in OCT have provided some correlations of the foveal microstructure with visual function in several retinal diseases.[9,16–19] Sekine, Imasawa and Iijima[9] reported that the thickness of the serous retinal detachment and not neurosensory retinal thickness, was significantly correlated with visual sensitivity measured by automated static perimetry in eyes with central serous chorioretinopathy. It was also reported that the initial VA was significantly worse in eyes with a higher serous retinal detachment in Vogt-Koyanagi-Harada disease but it was not significantly correlated with foveal thickness.[17] Therefore, we anticipated the possibility that some morphological parameters might be correlated with low luminance VA but this was not the case. Many factors such as the patient's age, duration of central serous chorioretinopathy, size of the detached area, central cone function and arrangement of cone and rod cells, may have influenced the low luminance VA.

There are some limitations of this study. The small sample might have limited the statistical power of our anlayses. Further investigation on the relationship between microstructural changes and low luminance VA would be helpful for understanding the pathologic mechanism of patients' complaints under reduced luminance conditions.

Studies of cases of unilateral central serous chorioretinopathy have shown that

the fellow eyes can have subclinical central serous chorioretinopathy. The studies of Maaranen, Tuppurainan and Mäntyjärvi[20] and Baran, Gürlü and Esgin[21] support this suggestion because they found a high percentage of colour deficiency in the fellow eyes of patients with central serous chorioretinopathy. Baran, Gürlü and Esgin[21] also observed that contrast sensitivity was reduced in the fellow eyes of patients with unilateral central serous chorioretinopathy. Iida and colleagues[22] reported choroidal vascular abnormalities in indocyanine green angiographic images in the unaffected fellow eye. In our study, the VA of fellow eyes was not significantly different from that of age-matched normal eyes. Further studies are needed to assess the visual status of fellow eyes.

In conclusion, the VA of eyes with central serous chorioretinopathy was significantly more depressed at low background luminances than normal eyes. Low background luminance VA testing is useful for evaluating visual disturbances at low ambient luminance experienced by patients with central serous chorioretinopathy. There is a potential use here as one of the functional parameters in evaluating and flagging of central serous chorioretinopathy or therapeutic effect of new therapies such as photodynamic therapy.

ACKNOWLEDGEMENT

Support of this study was provided by Researches on Sensory and Communicative Disorders from the Ministry of Health, Labor, and Welfare, Japan.

REFERENCES

1. Spaide RF, Campeas L, Haas A, Yannuzzi LA, Fisher YL, Guyer DR, Slakter JS et al. Central serous chorioretinopathy in younger and older adults. *Ophthalmology* 1996; 103: 2070–2079.
2. Gilbert CM, Owens SL, Smith PD, Fine SL. Long-term follow-up of central serous chorioretinopathy. *Br J Ophthalmol* 1984; 68: 815–820.
3. Norholm I. Central serous retinitis. A follow-up study. *Acta Ophthalmol* 1969; 47: 890–899.
4. Shlaer S. The relation between visual acuity and illumination. *J Gen Physiol* 1937; 21: 165–188.
5. Plainis S, Anastasakis AG, Tsilimbaris MK. The value of contrast sensitivity in diagnosing central serous chorioretinopathy. *Clin Exp Optom* 2007; 90: 296–298.
6. Marmor MF, Tan F. Central serous chorioretinopathy: bilateral multifocal electroretinographic abnormalities. *Arch Ophthalmol* 1999; 117: 184–188.
7. Miyake Y, Shiroyama N, Ota I, Horiguchi M. Local macular electroretinographic responses in idiopathic central serous chorioretinopathy. *Am J Ophthalmol* 1988; 106: 546–550.
8. Senturk F, Ozdemir H, Karacorlu M, Karacorlu SA, Uysal O. Microperimetric changes after intravitreal triamcinolone acetonide injection for macular edema due to central retinal vein occlusion. *Retina* 2010; 30: 1254–1261.
9. Sekine A, Imasawa M, Iijima H. Retinal thickness and perimetric sensitivity in central serous chorioretinopathy. *Jpn J Ophthalmol* 2010; 54: 578–583.
10. Kim SW, Oh J, Huh K. Correlations among various functional and morphological tests in resolved central serous chorioretinopathy. *Br J Ophthalmol* 2012; 96: 350–355.
11. Ojima Y, Tsujikawa A, Hangai M, Nakanishi H, Inoue R, Sakamoto A, Yoshimura N. Retinal sensitivity measured with the micro perimeter 1 after resolution of central serous chorioretinopathy. *Am J Ophthalmol* 2008; 146: 77–84.
12. Ozdemir H, Karacorlu SA, Senturk F, Karacorlu M, Uysal O. Assessment of macular function by microperimetry in unilateral resolved central serous chorioretinopathy. *Eye* 2008; 22: 204–208.
13. Hecht S. The resolution between visual acuity and illumination. *J Gen Physiol* 1928; 11: 255–281.
14. Chen B, MacLeod DI, Stockman A. Improvement in human vision under bright light: Grain or gain? *J Physiol* 1987; 394: 41–66.
15. Chuang EL, Sharp DM, Fitzke FW, Kemp CM, Holden AL, Bird AC. Retinal dysfunction in central serous retinopathy. *Eye* 1987; 1: 120–125.
16. Forte R, Cennamo G, Finelli M, Cesarano I, D'Amico G, De Crecchio G, Cennamo G. Intravitreal triamcinolone, bevacizumab and pegaptanib for occult choroidal neovascularization. *Acta Ophthalmol* 2010; 88: e305–e310.
17. Ikewaki J, Kimoto K, Choshi T, Nagata M, Motomura Y, Tamura K, Shinoda K et al. Optical coherence tomographic assessment of dynamic macular changes in patients with Vogt-Koyanagi-Harada disease. *Int Ophthalmol* 2010; 31: 9–13.
18. Geitzenauer W, Hitzenberger CK, Schmidt-Erfurth UM. Retinal optical coherence tomography: past, present and future perspectives. *Br J Ophthalmol* 2011; 95: 171–177.
19. Lim JW, Kang SW, Kim YT, Chung SE, Lee SW. Comparative study of patients with central serous chorioretinopathy undergoing focal laser photocoagulation or photodynamic therapy. *Br J Ophthalmol* 2011; 95: 514–517.
20. Maaranen TH, Tuppurainen KT, Mäntyjärvi MI. Color vision defects after central serous chorioretinopathy. *Retina* 2000; 20: 633–637.
21. Baran NV, Gürlü VP, Esgin H. Long-term macular function in eyes with central serous chorioretinopathy. *Clin Experiment Ophthalmol* 2005; 33: 369–372.
22. Iida T, Kishi S, Hagimura N, Shimizu K. Persistent and bilateral choroidal vascular abnormalities in central serous chorioretinopathy. *Retina* 2007; 19: 508–512.

Case Reports in Ophthalmology

Case Rep Ophthalmol
DOI: 10.1159/000339129

Published online:
■■■, 2012

ISSN 1663–2699
www.karger.com/cop

Case of Unilateral Peripheral Cone Dysfunction

Yujin Mochizuki[a] Kei Shinoda[b] Celso Soiti Matsumoto[b]
Gerd Klose[c] Emiko Watanabe[b] Keisuke Seki[b]
Itaru Kimura[a] Atsushi Mizota[b]

[a]Department of Ophthalmology, Juntendo University Urayasu Hospital, Chiba,
[b]Department of Ophthalmology, Teikyo University School of Medicine,
University Hospital Itabashi, and [c]Carl Zeiss Meditec Co., Ltd., Tokyo, Japan

Key Words
Tunnel vision · Electroretinogram · Multifocal ERG · Optical coherence tomography · Pattern visual evoked potentials

Abstract
Purpose: Peripheral cone dystrophy is a subgroup of cone dystrophy, and only 4 cases have been reported. We present a patient with unilateral peripheral cone dysfunction and report the functional changes determined by electrophysiological tests and ultrastructural changes determined by spectral domain optical coherence tomography (SD-OCT).
Case: A 34-year-old woman complained of blurred vision in both eyes. Our examination showed that her visual acuity was 0.05 OD and 0.2 OS. A relative afferent pupillary defect was present in her right eye. The results of slit-lamp examination, ophthalmoscopy, and fluorescein angiography were normal except for pallor of the right optic disc. SD-OCT showed a diffuse thinning of the retina in the posterior pole of the right eye. A severe constriction of the visual fields was found in both eyes but more in the right eye. The photopic full-field electroretinograms (ERGs) were reduced in the right eye but normal in the left eye. The multifocal ERGs were severely reduced throughout the visual field except in the central area of the right eye. The multifocal ERGs from the left eye were normal. The pattern visual evoked responses were within the normal range in both eyes. She had a 5-year history of sniffing paint thinner.
Results: Although the visual dysfunction was initially suspected to be due to psychological problems from the results of subjective tests, objective tests indicated a peripheral cone dysfunction in the right eye. The pathophysiological mechanism and the relationship with thinner sniffing were not determined.
Conclusions: Our findings indicate that peripheral cone dysfunction can occur unilaterally. Electrophysiology and SD-OCT are valuable tests to perform to determine the pathogenesis of unusual ocular findings objectively.

Kei Shinoda, MD

Department of Ophthalmology, Teikyo University School of Medicine
2-11-1 Kaga, Itabashi-ku, Tokyo 173-8605 (Japan)
Tel. +81 3 3964 1225, E-Mail shinodak@med.teikyo-u.ac.jp

Case Rep Ophthalmol
DOI: 10.1159/000339129
Published online: ■■■, 2012

ISSN 1663–2699
www.karger.com/cop

Introduction

An inherited central cone dysfunction was named occult macular dystrophy (OMD) or Miyake's disease [1–3], and the gene responsible for OMD has been identified [4]. In OMD, only the central cone function is abnormal. There are also cases where only the peripheral cone functions are abnormal while the central cone function is normal. However, these cases are rare and only four cases of peripheral cone dysfunction have been reported. In these cases, the rod function is normal over the entire retina [5, 6]. Kondo et al. [5] first described peripheral cone dystrophy, and they carefully analyzed focal areas of the central retina in 3 patients with peripheral cone dystrophy. They showed that the dysfunction of the cones was predominantly in the periphery and the central area was relatively well preserved. Okuno et al. [6] reported an elderly man with bilateral peripheral cone dystrophy, and the patient's signs and symptoms had not changed for over 50 years. Therefore they concluded that such condition in their case was not a manifestation of an early stage of the more common type of cone dystrophy.

We present a patient with peripheral cone dysfunction but the abnormalities were found in only one eye. In addition to the unilateral dystrophy, the patient had several features that were different from previous cases of peripheral cone dystrophy.

Case Report

A 34-year-old Japanese woman complained of a gradually decrease of her vision in both eyes. She visited a neighborhood eye clinic on December 2008, and the examination showed that her best-corrected decimal visual acuity (BCVA) was 0.3 OD and 0.5 OS. A diagnosis was not made, and she was not treated. Three months later she was referred to our clinic. She reported that she had noticed that her right visual field had been constricted for 10 years. She did not complain of photopsia, photophobia, night blindness, or color vision disturbances. She had a history of paint thinner sniffing of more than 5 years. Our examination showed that her BCVA was 0.05 OD and 0.2 OS. The results of slit-lamp biomicroscopy, ophthalmoscopy, and fluorescein angiography were normal except for right optic disc pallor (fig. 1). Goldman and Humphrey visual field tests showed a concentric constriction of the visual fields in both eyes but more severe in the right eye (fig. 1). A relative afferent pupillary defect was present in the right eye. Brain magnetic resonance imaging showed no abnormalities.

The amplitudes of the full-field scotopic b-waves of the ERGs were reduced in both eyes (fig. 2), and that of the mixed rod:cone ERGs were also reduced. The oscillatory potentials (OPs) and the photopic cone ERGs were unrecordable in the right eye, i.e., less than the noise level (5 μV for OPs and 20 μV for the photopic cone ERGs), and the flicker ERGs were highly attenuated by approximately 95% of that of the right eye. The responses from the left eye were essentially normal except that the amplitude of the scotopic rod ERGs was at the lower limit of the normal range.

The multifocal ERGs (mfERGs; fig. 2, online suppl. table 1; for all online suppl. material, see www.karger.com/doi/10.1159/000339129) were well preserved in the central retina but severely reduced in the periphery of the right eye. These findings were in good accordance with the results of perimetry. The mfERGs were well preserved in all areas of the left eye. The mfERGs from each concentric ring were summed and analyzed. This showed that only the central responses were preserved in the right eye, and no significant difference of the implicit time was found in the central area between the two eyes. Pattern visual evoked response was within normal limits in both eyes (fig. 2).

Microstructural images of the fovea were obtained by the SD-OCT (OCT4000, Cirrus HD-OCT, Carl Zeiss Medic Inc., Dublin, Calif., USA). The 3D datasets were obtained using the raster scan protocol of 128 horizontal B-scan images, each composed of 512 axial scans. This raster scan protocol covered an area of 6 mm (horizontal) × 6 mm (vertical) × 1.7 mm (axial) with a horizontal pixel spacing of 11 μm (6 mm/512) and a vertical pixel spacing of 47 μm (6 mm/128).

Case Rep Ophthalmol
DOI: 10.1159/000339129
Published online:
■■■, 2012

ISSN 1663–2699
www.karger.com/cop

High-quality images of 9 mm horizontal and 6 mm vertical scans were obtained using the HD 5-line raster scan protocol of 5 B-scan images, each composed of 1,024 axial scans. Each B-scan was aquired with 4-times oversampling and subsequent pixel profiling to obtain noise-reduced images. This raster scan protocol examines the cross section of B-scans through the fovea with a horizontal pixel spacing of 9 μm (9 mm/1,024) and a vertical pixel spacing of 6 μm (6 mm/1,024).

Based on the HD 5-line raster scans in the horizontal and vertical orientation of both the right and left eye, the outer nuclear layer (ONL) could be identified and its thickness determined. The thickness of the ONL was defined as the vertical distance between the highly reflective line corresponding to the external limiting membrane (ELM) and the midpoint of the transition from the highly reflective outer plexiform layer (OPL) to the less reflective ONL. Manual thickness measurements were made at many points on the central horizontal and vertical B-scan cross sections (online suppl. fig. 1) using the built-in caliper tool. In addition, the images were analyzed with the help of an external mathematical program to automatically detect the ONL boundaries and determine the layer thickness. The thickness values have been averaged over segments of 1 mm length, corresponding to the popular EDTRS grid.

In general, the configuration and microstructure in the macula were normal in both eyes; the ELM, the photoreceptor inner and outer segment (IS/OS) lines, and the foveal bulge were distinct in the SD-OCT images in both eyes (fig. 1). However, comparisons of each layer between the two eyes showed a diffuse thinning of the retina especially the ONL in the extramacular area of the right eye. Online supplementary table 2 summarizes the quantitative results obtained from the manual and automated thickness analysis.

Discussion

Peripheral cone dystrophy is a very rare clinical entity, and its clinical characteristics have been presented in only two publications [5, 6]. The possibility of having patients with peripheral cone dystrophy or patients with similar characteristics has been discussed [7–10]. However, these authors did not compare the central and peripheral cone function and also did not demonstrate that the rod system was functioning normally across the retina.

Recent developments of the clinical techniques of evaluating retinal function in localized areas, e.g., focal ERGs, mfERGs, and rod and cone perimetry, have allowed assessments of central [1–3] or peripheral cone dysfunction [5, 6]. The etiology of the findings of our case is unknown. Inherited diseases, vascular disease, systemic disease, infection, inflammation, and an exposure to toxins were considered in the differential diagnosis. Our case had a history of paint thinner sniffing, and thus the results of subjective testing should be carefully interpreted. However, the electrophysiological findings including full-field ERGs, mfERGs, and visual evoked potentials clearly showed diffuse cone dysfunction except in the central area of only the right eye. On the other hand,rod in the right eye, both rod and cone in the left eye, and optic nerve functioned well in both eyes. Moreover microstructural analysis on the retina supports these objective functional results. However, the severely decreased visual acuity and highly constricted visual field in both eyes do not agree with our diagnosis of peripheral cone dystrophy. These contradictory findings might be because our patient had psychogenic disorders induced by thinner sniffing and the possibility of unilaterally pronounced toxic effects cannot be denied [11]. But thinner sniffing has been reported to lead to mainly optic neuropathy [12, 13] but the normal visual evoked potentials of our patient indicated that this was not likely.

Another differential diagnosis of our case is acute zonal occult outer retinopathy (AZOOR) which is a uni- or bilateral disease characterized by an acute zonal loss of

Case Rep Ophthalmol
DOI: 10.1159/000339129
Published online:
■■■, 2012

ISSN 1663–2699
www.karger.com/cop

outer retinal function with minimal ophthalmoscopic changes [14]. Recently, local retinal microstructure assessed by Fourier-domain and spectral-domain optical coherence tomography showed that the major OCT findings in this disease were the selective absence or discontinuity of the IS/OS line and the cone outer segment tip (COST) line in the retinal areas corresponding to the functional decrease [15, 16]. Defect of the IS/OS line and thinning of the ONL has been reported in AZOOR [17, 18]. In our case, the onset was not acute according to the patient's description, but otherwise the clinical manifestations are compatible to AZOOR clinical entity. However, we believe that our case was not AZOOR because the IS/OS line appeared normal in the area with severely reduced mfERGs in the right eye, and a unilateral, diffuse, peripheral, cone-selective dysfunction in AZOOR has not been reported.

Microstructural analyses showed a selective thinning of the ONL with the outer plexiform layer and IS/OS line intact. These findings are in good agreement with the severe attenuation of the a-wave in photopic ERG and mfERG. This supports the idea of a selective cone dysfunction.

Only five cases of unilateral cone dysfunction have been reported [19–22]. Two cases from Sieving [19] had normal rod ERGs in both eyes but reduced cone ERGs in only one eye. He reported abnormally prolonged b-wave when long-duration photopic flashes were used, and these abnormalities were ascribed to the hyperpolarizing bipolar and/or horizontal cells. In contrast, our subject had no measurable full-field photopic ERGs. The other three cases, a 19-year-old woman reported by Zervas and Smith [20], a 53-year-old woman by Brigell and Celesia [21], and a 20-year-old woman by Nomura et al. [22], had unilateral severe cone dysfunction while the rod function was intact in both eyes, which is similar with our case. But all three cases had an acute onset and the 20-year-old woman demonstrated bull's eye maculopathy three months later. The two cases from Zervas and Smith, and Brigell and Celesia had good visual acuity and ophthalmoscopically normal macula in the affected eye. Although information about focal macular ERGs was not reported in these cases, the abnormal full-field ERGs and preserved macular function appear similar to our case, except that our case had severely reduced visual acuity.

Considering all of our findings, we conclude that our case had unilateral peripheral cone dysfunction, and the findings are different from those of the more common cone dystrophy as well as of the reported cases with peripheral cone dystrophy.

Disclosure Statement

No author has a financial or proprietary interest in any material or method mentioned except that G.K. is employed at Carl Zeiss Meditec Co., Ltd., Japan (support limited to not-commercially available data analysis). Support of this study was provided by Research Grants on Sensory and Communicative Disorders from the Ministry of Health, Labor, and Welfare, Japan.

Case Rep Ophthalmol
DOI: 10.1159/000339129
Published online:
■■■, 2012
© 2012 S. Karger AG, Basel
ISSN 1663–2699
www.karger.com/cop

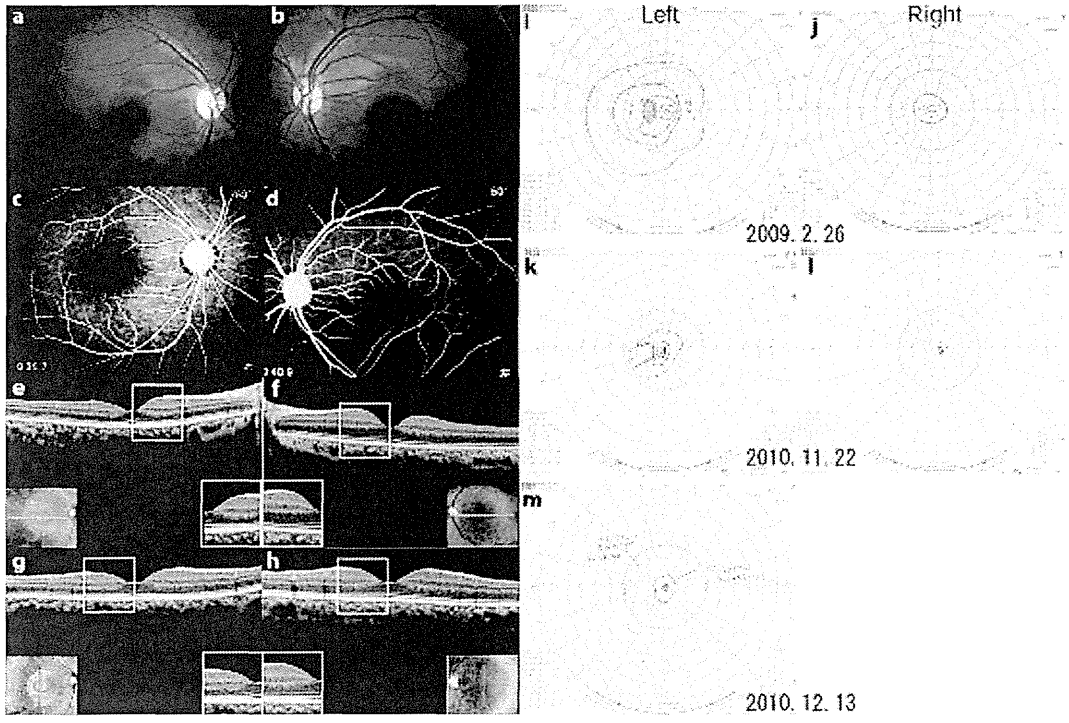

Fig. 1. Fundus photographs, fluorescein angiograms, visual fields, and optical coherence tomographic (OCT) images from our patient with unilateral peripheral cone dystrophy. **a–d** Fundus photographs and fluorescein angiograms showing no abnormal findings. **e–h** OCT images from a 9-mm horizontal scan of the right (**e**) and left (**f**) eyes and vertical scan in the right (**g**) and left (**h**) eyes. Note that the outer nuclear layer is thinner in the right eye than that in the left eye in large areas of the retinal except the fovea (**inset**). **i–m** Goldmann visual fields showing bilateral constriction of the visual fields in both eyes but more severe in the right eye.

Case Rep Ophthalmol
DOI: 10.1159/000339129
Published online:
■■■, 2012

ISSN 1663–2699
www.karger.com/cop

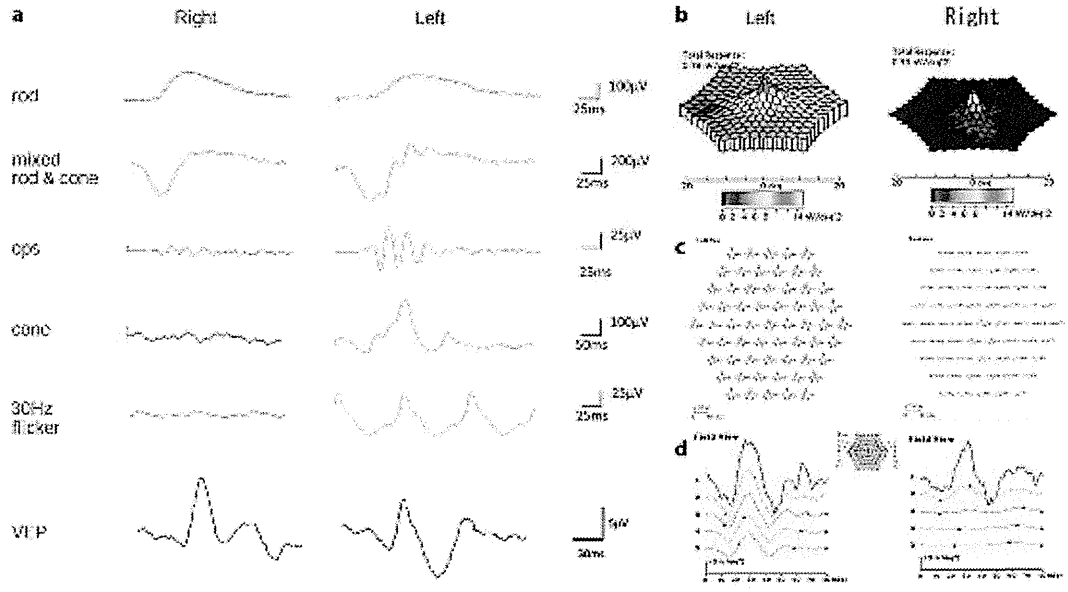

Fig. 2. Full-field and multifocal electroretinograms (ERGs) recorded from our patient with unilateral peripheral cone dystrophy. Full-field ERG showed that rod responses are symmetrical in both eyes, but the responses of cone system are flat in the right eye while normal in the left eye. The multifocal ERGs are severely attenuated in the peripheral retinal area while that from the central area is normal in the right eye. The response density in the left eye was normal.

References

1 Miyake Y, Ichikawa K, Shiose Y, Kawase Y: Hereditary macular dystrophy without visible fundus abnormality. Am J Ophthalmol 1989;108:292–299.

2 Miyake Y, Horiguchi M, Tomita N, Kondo M, Tanikawa A, Takahashi H, Suzuki S, Terasaki H: Occult macular dystrophy. Am J Ophthalmol 1996;122:644–653.

3 Miyake Y: Electrodiagnosis of Retinal Disease. Tokyo, Springer-Verlag, 2006.

4 Akahori M, Tsunoda K, Miyake Y, Fukuda Y, Ishiura H, Tsuji S, Usui T, Hatase T, Nakamura M, Ohde H, Itabashi T, Okamoto H, Takada Y, Iwata T: Dominant mutations in RP1L1 are responsible for occult macular dystrophy. Am J Hum Genet 2010;87:424–429.

5 Kondo M, Miyake Y, Kondo N, Ueno S, Takakuwa H, Terasaki H: Peripheral cone dystrophy: a variant of cone dystrophy with predominant dysfunction in the peripheral cone system. Ophthalmology 2004;111:732–739.

6 Okuno T, Oku H, Kurimoto T, Oono S, Ikeda T: Peripheral cone dystrophy in an elderly man. Clin Experiment Ophthalmol 2008;36:897–899.

7 Krill AE, Deutman AF, Fishman M: The cone degenerations. Doc Ophthalmol 1973;35:1–80.

8 Pinckers A, Deutman AF: Peripheral cone disease. Ophthalmologica 1977;174:145–150.

9 Pearlman JT, Owen WG, Brounley DW, Sheppard JJ: Cone dystrophy with dominant inheritance. Am J Ophthalmol 1974;77:293–303.

10 Noble KG, Siegel IM, Carr RE: Progressive peripheral cone dysfunction. Am J Ophthalmol 1988;106:557–560.

11 Toyonaga N, Adachi-Usami E, Yamazaki H: Clinical and electrophysiological findings in three patients with toluene dependency. Doc Ophthalmol 1989;73:201–207.

12 Kohriyama K, Hori H, Murai Y, Ninomiya H, Tsukamoto Y: Optic neuropathy induced by thinner sniffing. J UOEH 1989;11:449–453.

13 Poblano A, Lope Huerta M, Martínez JM, Falcón HD: Pattern-visual evoked potentials in thinner abusers. Arch Med Res 1996;27:531–533.

14 Gass JD: Acute zonal occult outer retinopathy. Donders Lecture: The Netherlands Ophthalmological Society, Maastricht, Holland, June 19, 1992. J Clin Neuroophthalmol 1993;13:79–97.

15 Park SJ, Woo SJ, Park KH, Hwang JM, Chung H: Morphologic photoreceptor abnormality in occult macular dystrophy on spectral-domain optical coherence tomography. Invest Ophthalmol Vis Sci 2010;51:3673–3679.

16 Sugahara M, Shinoda K, Matsumoto CS, Satofuka S, Hanazono G, Imamura Y, Mizota A: Outer retinal microstructure in a case of acute idiopathic blind spot enlargement syndrome. Case Report Ophthalmol 2011;2:116–122.

17 Spaide RF, Koizumi H, Freund KB: Photoreceptor outer segment abnormalities as a cause of blind spot enlargement in acute zonal occult outer retinopathy-complex diseases. Am J Ophthalmol 2008;146:111–120.

18 Ohta K, Sato A, Fukui E: Spectral domain optical coherence tomographic findings at convalescent stage of acute zonal occult outer retinopathy. Clin Ophthalmol 2009;3:423–428.

19 Sieving PA: Unilateral cone dystrophy: ERG changes implicate abnormal signaling by hyperpolarizing bipolar and/or horizontal cells. Trans Am Ophthalmol Soc 1994;92:459 –471; discussion 471–474.

20 Zervas JP, Smith JL: Neuro-ophthalmic presentation of cone dysfunction syndromes in the adult. J Clin Neuroophthalmol 1987;7:202–218.

21 Brigell M, Celesia GG: Electrophysiological evaluation of the neuro-ophthalmology patient: an algorithm for clinical use [review]. Semin Ophthalmol 1992;7:65–78.

22 Nomura R, Kondo M, Tanikawa A, Yamamoto N, Terasaki H, Miyake Y: Unilateral cone dysfunction with bull's eye maculopathy. Ophthalmology 2001;108:49–53.

Stiles–Crawford effect in focal macular ERGs from macaque monkey

Celso Soiti Matsumoto — Department of Ophthalmology, Faculty of Medicine, Oita University, Oita, Japan, Department of Ophthalmology, Teikyo University School of Medicine, Tokyo, Japan, & Matsumoto Eye Clinic, Tokushima, Japan

Kei Shinoda — Department of Ophthalmology, Teikyo University School of Medicine, Tokyo, Japan

Harue Matsumoto — Matsumoto Eye Clinic, Tokushima, Japan

Shingo Satofuka — Department of Ophthalmology, Teikyo University School of Medicine, Tokyo, Japan

Atsushi Mizota — Department of Ophthalmology, Teikyo University School of Medicine, Tokyo, Japan

Kazuo Nakatsuka — Shonin Hospital, Oita, Japan

Yozo Miyake — Aichi Medical University, Aichi, Japan

Background: To determine whether the focal macular electroretinograms (FMERGs) are affected by the angle of incidence of the stimulating light on the retina, i.e., the Stiles–Crawford effect (SCE). *Methods*: FMERGs were elicited by focal stimulation of the macula in three light-adapted macaque monkeys. The incidence of the light on the retina was varied from 0 to ±11.7°. The effects of the incidence and wavelengths of the stimulus on the SCE were determined. *Results*: The amplitudes of the FMERG components were largest when the stimulus beam entered the eye on the visual axis and passed through the center of the pupil. The amplitudes gradually decreased as the stimulus beam passed through the pupil more eccentrically and fell on the retina more obliquely. All components of the FMERGs were decreased with the decrease least for the amplitude of the d-wave. *Conclusions*: The decrease in the amplitudes of the FMERGs as the angle of incidence of the stimulus beam on the retina increases demonstrates that the SCE can be detected in adult macaque monkeys. This objective method of assessing the SCE suggests that this technique can be used to assess the alignment of cones in humans with different types of macular diseases.

Keywords: Stiles–Crawford effect, focal macular electroretinogram, ERG

Citation: Matsumoto, C. S., Shinoda, K., Matsumoto, H., Satofuka, S., Mizota, A., Nakatsuka, K., & Miyake, Y. (2012). Stiles–Crawford effect in focal macular ERGs from macaque monkey. *Journal of Vision, 12*(3):6, 1–7, http://www.journalofvision.org/content/12/3/6, doi:10.1167/12.3.6.

Introduction

Focal macular electroretinograms (FMERGs) have been used to assess the physiological condition of different retinal neuronal cells including the photoreceptors in the macular area (DeLint, Berendschot, & van Norren, 1998; Kondo, Miyake, Horiguchi, Suzuki, and Tanikawa, 1998). In most experimental and clinical studies, FMERGs have been recorded, and the effects of the Stiles–Crawford effect (SCE), a decrease in the luminous efficiency of light entering the edge of the pupil, were not examined. However with focal stimulation, the direction of the incidence beam becomes more important.

Evidence has been obtained that the directional sensitivity of the cones to light stimuli is responsible for the SCE (Alpern, 1986; Alpern, Kitahara, & Fielder 1987; Alpern & Kitahara, 1983; Stiles & Crawford, 1933). The SCE is generally determined by psychophysical tests (Alpern, 1986; Alpern et al., 1987; Alpern & Kitahara, 1983; DeLint, Vos, Berendoschot, & van Norren, 1997), and the subjects are required to actively participate in the examination. Thus, high level of concentration and good visual acuity are required to perform the tests.

doi: 10.1167/12.3.6 Received June 11, 2011; published March 6, 2012 ISSN 1534-7362 © ARVO

The SCE has been examined objectively in humans by only a few investigators. DeLint et al. analyzed the SCE by measuring the visual pigment density with different incidences of the bleaching and reflected light (DeLint et al., 1998). Birch et al. stimulated focal macular areas with a steady-state flickering light through a two-channel Maxwellian-view optical system to elicit focal ERGs (Birch, Sandberg, & Berson, 1982). They showed that the SCE could be demonstrated at the fovea in normal subjects. However, they isolated the b-waves by using band-pass filters, and a separation of a-wave and d-wave components was not possible. The FMERGs in our study enabled us to isolate the a-, b-, and d-waves, and we were able to analyze each component to determine whether each showed the SCE effect.

We have developed an FMERG system that is integrated into a slit lamp that allowed us to stimulate the retina with a spot of light at any incidence (Choshi, Matsumoto, & Nakatsuka, 2003; Yamada, Matsumoto, & Nakatsuka, 2006). This FMERG stimulating and recording system prompted us to assess the SCE objectively with long-duration stimuli. This system allowed the ERG recordings to be performed under direct fundus observation, and each component of the FMERGs could be analyzed separately.

Thus, the purpose of this study was to determine whether the SCE was present in the foveal area of macaque monkeys. To accomplish this, we elicited FMERGs from three macaque monkeys by light of different incidences on the retina. We shall show that all components of the FMERGs were affected by the SCE with the d-wave least affected.

Materials and methods

Animals

Focal macular ERGs (FMERGs) were recorded from 3 eyes of 3 adult (ages 6, 6, and 8 years) male macaque monkeys (*Macaca fuscata*). All experimental and animal care procedures adhered to the ARVO Statement for the Use of Animals in Ophthalmic and Vision Research and were approved by the Institutional Animal Care Committee of Oita University.

FMERG recordings

The monkeys were initially anesthetized by an intramuscular injection of a mixture of ketamine (7 mg/kg), xylazine (0.6 mg/kg), and butorphanol tartrate (0.04 mg/kg) and maintained on an infusion of the same proportions of ketamine, xylazine, and butorphanol tartrate per hour. The depth of the anesthesia was maintained at a level sufficient to inhibit the corneal reflex and eye movements. The pupils were dilated with topical tropicamide (0.5%) and phenylephrine hydrochloride (5%), and the cornea was anesthetized with topical oxybuprocaine hydrochloride (0.4%). The non-stimulated eye was covered with an opaque patch.

Photopic stimuli

An optical system was built to deliver focal stimuli to the macula under direct fundus observation. The system was designed so that the stimulus light passed through the center of the pupil, i.e., on the visual axis, or through different parts of the pupil from the temporal to nasal edge in 0.5-mm steps. The light sources were from hyper-bright light-emitting diodes (LEDs; NSPW500BS, NICHIA, Tokushima, Japan), and the stimuli positioning unit was a motorized helicoid stage (Sigma Koki, Saitama, Japan) with a telescopic optical system mounted on the stage. The stage moved the telescope so that the stimulating beam entered the pupil from the temporal to nasal sides across the visual axis in 0.5-mm steps. The movement of the stage had an accuracy of 0.05 mm.

The fundus observation system was composed of a near-infrared CCD camera (Hitachi, Japan) integrated on a customized slit lamp microscope (Carl-Zeiss, Germany). The position of the light spot on the macular area was monitored during all of the recordings. The stimulus spot was 5° in diameter. To examine the effects of the wavelength of the stimulus on the SCE, red (λ_{max} = 644 nm, half-amplitude bandwidth of 634 to 655 nm, TLRH180P, TOSHIBA, Tokyo, Japan), amber (λ_{max} = 590 nm, half-amplitude bandwidth of 585 to 596 nm, TLYE260A, TOSHIBA, Tokyo, Japan), green (λ_{max} = 523 nm, half-amplitude bandwidth of 512 to 545 nm, SLA580EC4T, ROHM, Kyoto, Japan), and blue (λ_{max} = 470 nm, half-amplitude bandwidth of 460 to 482 nm, NSPB500S, NICHIA, Tokushima, Japan) LEDs were used to elicit the FMERGs.

The white light stimulus intensity was set to 38 cd/m^2. The spectral characteristics (bandwidth and λ_{max}) of the LEDs used in this study were measured with a spectral colorimeter PR-650 SpectraScan and analyzed with SpectraView software (Photoresearch, CA, USA).

To determine whether the ERGs were focal, the 5° stimulus spot was projected onto the optic nerve head, and FMERGs were elicited by decreasing stimulus intensities. The FMERGs recorded by the stimulus projected on the optic nerve head became non-recordable when the intensity was ≤38 cd/m^2 indicating that this stimulus intensity would provide a focal response from the macula with negligible effect of stray light (Choshi et al., 2003; Yamada et al., 2006). The intensity of each colored light stimulus was matched by neutral density filters to elicit approximately the criteria amplitude of b-wave (1 μV) as elicited by the white stimulus whose luminance was

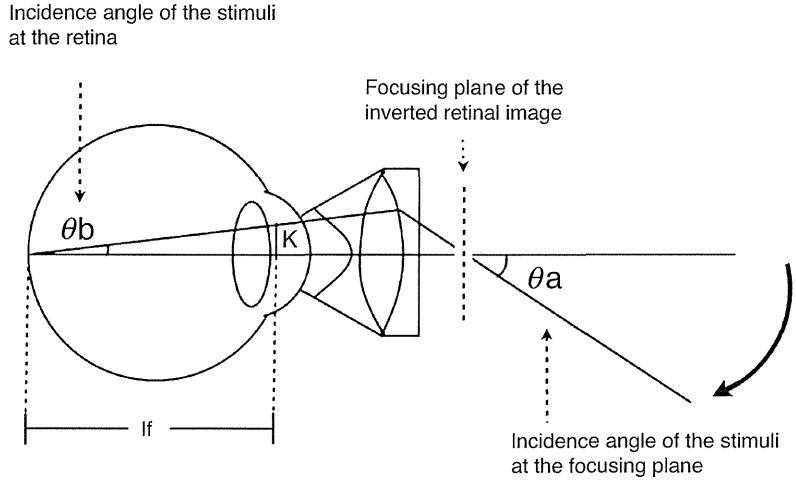

Figure 1. Relationship between the angle of incidence of the light beam on the focusing plane of the inverted retinal image. IF = IF distance, i.e., the axial length minus the corneal thickness and anterior chamber depth and K = distance of the stimulus beam from the visual axis in the iris plane in millimeters.

$\leq$38 cd/m^2. The FMERG waveforms were comprised of on and off waves. The adjusted intensity elicited no ERGs when the stimulus spot was projected onto the optic nerve head.

A gold-foil bipolar contact lens (Mayo, Nagoya, Japan) coupled with a mini-pan fundus lens was placed on the cornea of the examined eye (Figure 1). This provided an inverted real image of the ocular fundus projected approximately 3.5 mm in front of the contact lens unit. The relationship between the angle of incidence of the light beam on the focusing plane of the inverted retinal image and that on the retinal surface was calculated as shown in Figure 1. When the light beam fell on the temporal side of the real image at an angle of θ_a, then the light beam will be projected from the nasal side onto the retinal surface at an angle of θ_b. The relationship between θ_a and θ_b was calculated by

$$[\tan\theta_b = C(\tan\theta_a)], \quad (1)$$

with θ_b being the angle of incidence on the retina, θ_a being the angle of incidence on the focusing plane of the inverted retinal image, and C being the lens magnification constant. Thus, θ_b was determined by the telescope angle and C by the lens magnification constant (0.39).

The distance between the center of the pupil and the stimulus beam was measured as shown in Figure 1. The iris–fovea distance, IF, was calculated by

$$\mathrm{IF} = K/(\tan\theta_b), \quad (2)$$

with K equal to the distance of the light beam from the visual axis in the iris plane, and IF equal to the distance of the axial length with the subtraction of corneal thickness and the anterior chamber depth. A correction for light transmission through the cornea and the lens was not done. The axial length, corneal thickness, and the anterior chamber depth were measured by A-mode ultrasound echography (Compuscan LT, Stortz, St. Louis, MO, USA).

The stimulus duration was 100 ms and the stimulus interval was 150 ms, and thus, the frequency of stimulation was 4 Hz. This stimulus pattern of 100 ms on and 150 ms off was used for each wavelength stimulus. A white light of 35 cd/m^2 for 15 min was used for light adaptation before recording with each wavelength. We believe that the off duration was long enough because the depolarization of the cone is much faster than 150 ms.

FMERG recordings and analyses

A bipolar contact lens electrode (Mayo, Nagoya, Japan) was used to pick up the FMERGs. The ground electrode was attached to the right ear lobe. After centering and focusing the stimulus spot on the macula, the eye was light adapted with 35 cd/m^2 for 15 min. Then, the FMERGs were elicited by different stimulus intensities and wavelengths. The responses were amplified with a NeuropackΣ bioamplifier (MEB-5500, Nihon Kohden, Tokyo), A/D converted at 16 bits (PCI-16/16UD, Contec, Japan), and averaged by a customized signal processing program (MTS, Japan). More than forty responses were averaged, and the sampling rate was 10 kHz (every 0.1 ms). The responses were filtered from 0.5 to 200 Hz with a hardwired band-pass filter. With this system, the noise level with the electrode placed on the cornea and no stimulus was less than 0.1 μV.

The amplitude of the a-wave was measured from the baseline to the trough of the a-wave, and the amplitude of the b-wave was measured from the trough of the a-wave

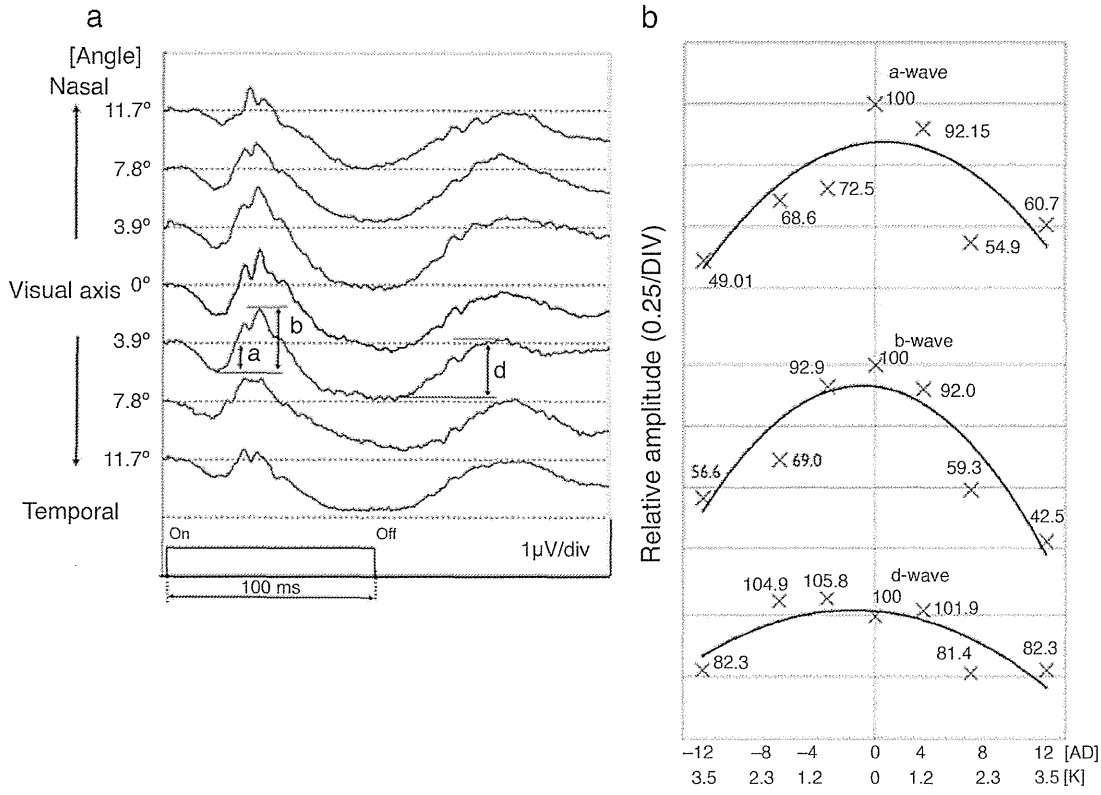

Figure 2. (a) Representative FMERGs elicited by white stimuli entering the pupil at different distances (ordinate) from the visual axis (0) for up to 11.7 degrees. The amplitudes of the a- and b-waves of the FMERGs decrease with increasing distance from the visual axis. (b) The amplitudes of the a-, b-, and d-waves were measured from ERGs such as those from the three monkeys, and the relative amplitudes are plotted on the right. One division of the graph is equal to 25%. *K* represents the distance of the entrance beam to the visual axis in the iris plane in millimeters; AD represents the mean angle of incidence in degrees of stimulus spot from the axis. The blue LED has a peak at 470 nm with a half-amplitude bandwidth between 442 and 520 nm. The green LED has a peak at 523 nm with a half-amplitude bandwidth between 480 and 620 nm. The yellow–orange LED has a peak at 590 nm with a half-amplitude bandwidth between 470 and 620 nm. The red LED has a peak at 644 nm with a half-amplitude bandwidth between 580 and 675 nm.

to the following positive peak (Figure 2). The amplitude of the d-wave was measured from the trough just preceding the d-wave to the positive peak after the stimulus offset.

All of the results are expressed as means ± standard deviations (*SD*s). The polynomial fit of the data was made with the Excel program, ver. 12.0. The polynomial fit was at order 2 for all data.

Results

The amplitudes of the a- and b-waves of the FMERGs were largest when the stimulus beam entered the eye on the visual axis (K = 0 mm, retinal angular incidence = 0 degree), and they decreased progressively as the stimulus beam entered more eccentrically up to the edge of the pupil. For example with white light, the average (n = 3) relative amplitude of the a-wave at 11.7° was approximately one-half of that at 0°. In the same way, the average (n = 3) of the relative amplitude of the b-wave at 11.7° was approximately one-half of that at 0°. Similar changes were found for the d-wave although the degree of change (reduced by 17.7 to 18.6%) was smaller (Figure 2 and Supplementary Table 1). With other wavelengths, the changes depended on the stimulus angle, but the relative amplitude of the d-wave was not evident.

The relative amplitudes of the FMERGs elicited by different wavelengths with peak transmission at 470 nm, 524 nm, 590 nm, and 644 nm are shown in Figure 3. As with the white stimuli, the amplitudes of the a- and b-waves were largest when the light beam entered the pupil on the visual axis and decreased with greater eccentricities. However, the degree of the SCE was not significantly affected by the wavelength of the stimuli (Figure 3).

When the relative amplitude difference was compared between the b-wave and d-wave, significant differences were found for each wavelength used. The relative amplitude differences was calculated as the relative amplitude by the stimulus at 0K—that by the stimulus at

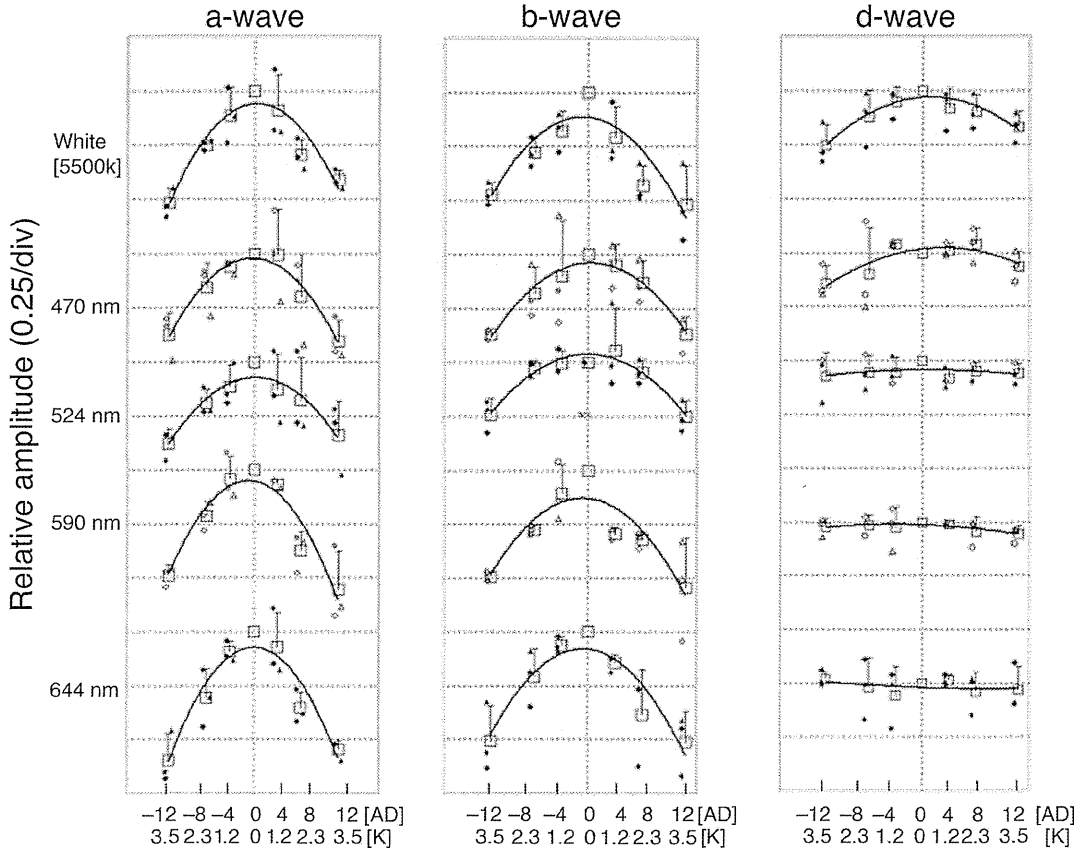

Figure 3. Relative amplitudes of the a-, b-, and d-waves elicited by different wavelengths of the stimulus. The λ_{max} of the stimuli was at 470 nm, 524 nm, 590 nm, and 644 nm. The small symbols (circles, triangles, and asterisks) represent the individual monkeys, the large squares are the averages, and the bars are the standard error of the means. One division of the graph is equal to 25%. *K represents the mean distance of the entrance beam to the visual axis in the iris plane in millimeters; †AD represents the mean angle of incidence in degrees of stimulus spot from the axis.

3.5K (Supplementary Table 1). The relative amplitude difference between maximal incidence stimuli and minimal incidence stimuli was significantly larger for the b-wave than for the d-wave for all wavelengths (Supplementary Table 1). Thus, the d-wave amplitude at the maximal stimulus incidence did not decrease as much as that of the b-wave suggesting that the SCE was larger for the b-waves than for the d-waves.

Discussion

Our results showed that the amplitudes of the a-wave and b-waves of the FMERGs were largest when the stimulus beam entered the eye through the center of the pupil and struck the retina perpendicularly. The amplitudes decreased progressively with increasing eccentricities of the stimulus beam. This is comparable to the SCE obtained psychophysically, and our results demonstrated that the SCE can be measured objectively using the FMERGs to assess the response of the retina.

The SCE is based on the ability of the photoreceptors to absorb photons passing through the outer segments, and the chances of a photon striking a photopigment increase when the beam passes perpendicularly through the entire extent of the outer segments. This explains why the FMERGs are largest when the stimulating beam entered the eye along the visual axis.

More than 25 years earlier, Birch et al. (1982) showed that the SCE can be demonstrated in the focal ERGs elicited by flickering stimuli obtained from a two-channel Maxwellian-view optical system. Our results confirmed their findings and also provided new information on the characteristics of the different components of the ERG and the influence of the wavelength of stimulating light.

Our data showed a drop-off in amplitude of the FMERGs when elicited by stimuli entering the edge of the pupil was approximately 50% whereas it was reported that the decrease of sensitivity was 1 log unit psychophysically (Alpern & Kitahara, 1983) or by OCT (Gao, Cense, Zhang, Jonnal, & Donald, 2008). The discrepancy between perimetry or OCT and the FMERGs is most likely due to methodological differences, i.e., the

FMERGs were elicited by suprathreshold stimulus intensities from focal areas, whereas perimetry employs near threshold stimuli. The FMERGs sum the activity of all of activated cells in the retina, whereas the psychophysical threshold is determined by the activity of the most sensitive cells. An alternative explanation might be that the differences were due to the differences in the species studied.

The degree of the SCE was similar for the a- and b-waves but lower for the d-wave. The origin of each wave is thought to be different. The a- and b-waves receive input from postreceptoral cells including off bipolar cells (Bush & Sieving, 1994) and from on bipolar cell (Sieving, Murayama, & Naarendorp, 1994), respectively. The d-wave arises from the activity of both the photoreceptors and inner retinal neurons (Sieving et al., 1994).

The difference may be due to the distribution of the different types of cones in the macular area (Yamamoto, Gouras, & Lopez, 1995). Another and more likely explanation is that the difference arises from the complexity of the ERG responses with several ERG components interacting. The d-waves of the full-field ERGs result from an interaction of the cone photoreceptor recovery and on bipolar offset and off bipolar cell depolarization. For focal stimuli, the response might be complicated by the photopic negative response (PhNR), because the d-wave is abolished by TTX treatment (Kurimoto et al., 2009; Yamada et al., 2006). Further investigations must be done to determine the reason for the different properties of the d-waves.

Stiles (1937) showed that the SCE depended on the wavelength of the light stimuli, and Alpern and Kitahara (1983) demonstrated that the directional sensitivity parameter (P) is dependent on the wavelength, namely, P was high at short (400 nm) and long (700 nm) wavelengths and lower at middle (550 nm) wavelengths. Our methods were not sensitive enough to detect these differences for the different wavelengths of the stimuli, probably because the bandwidths of the stimuli were relatively broad in our study. This was a limitation of the FMERGs. We used 4 LEDs with different wavelength and white light, while Alpern and Kitahara used 30 different monochromatic stimuli. Although each LED provides irradiance with relative steep peak, the relative broad bandwidth in our study might reduce the sensitivity to determine the difference depending on the stimulus wavelength. Using shorter, e.g., 400 nm, and longer, e.g., 700 nm, wavelength stimuli might have increased the sensitivity.

In conclusion, our results showed that the SCE can be determined objectively by the FMERGs. They also indicate that the SCE must be considered in interpreting the results of electrophysiological studies, particularly when focal stimuli are used to assess the macular area. Because the SCE is dependent on the passage of light through the outer segments of the photoreceptors, the FMERGs can be used to examine the alignment and integrity of the photoreceptors of the fovea in different types of macular diseases.

Acknowledgments

Support of this study was provided by Researches on Sensory and Communicative Disorders from the Ministry of Health, Labor, and Welfare, Japan. No author has a financial or proprietary interest in any material or method mentioned.

Commercial relationship: none.
Correspondence: Kei Shinoda, M.D., Ph.D.
Email: shinodak@med.teikyo-u.ac.jp.
Address: Department of Ophthalmology, Teikyo University School of Medicine, Kaga 2-11-1, Itabashi-ku, Tokyo 173-8605, Japan.

References

Alpern, M. (1986). The Stiles–Crawford effect of the second kind (SCII): A review. *Perception, 15,* 785–799.

Alpern, M., Kitahara, H., & Fielder, G. H. (1987). The change in color matches with retinal angle of incidence of the colorimeter beams. *Vision Research, 27,* 1763–1778.

Alpern, M., & Kitahara, K. (1983). The directional sensitivities of the Stiles' colour mechanisms. *The Journal of Physiology, 338,* 627–649.

Birch, D. G., Sandberg, M. A., & Berson, E. L. (1982). The Stiles–Crawford effect in retinitis pigmentosa. *Investigative Ophthalmology & Visual Science, 22,* 157–164.

Bush, R. A., & Sieving, P. A. (1994). A proximal retinal component in the primate photopic ERG a-wave. *Investigative Ophthalmology & Visual Science, 35,* 635–645.

Choshi, T., Matsumoto, C. S., & Nakatsuka, K. (2003). Rod-driven focal macular electroretinogram. *Japanese Journal of Ophthalmology, 47,* 356–361.

DeLint, P. J., Berendschot, T. T., & van Norren, D. (1998). A comparison of the optical Stiles–Crawford effect and retinal densitometry in a clinical setting. *Investigative Ophthalmology & Visual Science, 39,* 1519–1523.

DeLint, P. J., Vos, J. J., Berendschot, T. T. & van Norren, D. (1997). On the Stiles–Crawford effect with age. *Investigative Ophthalmology & Visual Science, 38,* 1271–1274.

Gao, W., Cense, B., Zhang, Y., Jonnal, R. S., & Donald, T. M. (2008). Measuring retinal contributions to the optical Stiles–Crawford effect with optical coherence tomography. *Optics Express, 16,* 6486–6501.

Kondo, M., Miyake, Y., Horiguchi, M., Suzuki, S., & Tanikawa, A. (1998). Recording multifocal electroretinogram on and off responses in humans. *Investigative Ophthalmology & Visual Science, 39,* 574–580.

Kurimoto, Y., Kondo, M., Ueno, S., Sakai, T., Machida, S., & Terasaki, H. (2009). Asymmetry of focal macular photopic negative responses (PhNRs) in monkeys. *Experimental Eye Research, 88,* 92–98.

Sieving, P. A., Murayama, K., & Naarendorp, F. (1994). Push–pull model of the primate photopic electroretinogram: A role for hyperpolarizing neurons in shaping the b-wave. *Visual Neuroscience, 11,* 519–532.

Stiles, W. S. (1937). The luminous efficiency of monochromatic rays entering the eye pupil at different points and a new colour effect. *Proceedings of the Royal Society of London B: Biological Sciences, 137,* 90–118.

Stiles, W. S., & Crawford, B. H. (1933). The luminous efficiency of rays entering the eye pupil at different points. *Proceedings of the Royal Society of London B: Biological Sciences, 112,* 428–450.

Yamada, K., Matsumoto, C. S., & Nakatsuka, K. (2006). Effect of spatial frequency of stimulus on focal macular ERGs in monkeys. *Documenta Ophthalmologica, 113,* 83–91.

Yamamoto, S., Gouras, P., & Lopez, R. (1995). The focal cone electroretinogram. *Vision Research, 35,* 1641–1649.

Novel Mutations in Enhanced S-cone Syndrome

Dear Editor:

Enhanced S-cone syndrome (ESCS) is a rare and unique retinal dystrophy with a pattern of autosomal-recessive inheritance.[1-3] Patients with ESCS show night blindness and high sensitivity to short-wavelength light, because of the 2-fold increased number of short-wavelength-sensitive cones (S cones) with absence of rods in the retina. Since the first discovery of mutations in the *NR2E3* gene on chromosome 15q23 in patients with ESCS,[4] >40 mutations have been reported as causes of ESCS and allied diseases (Fig 1, available online at http://aaojournal.org).

In this letter, we report novel mutations in the *NR2E3* gene that were discovered in 2 cases with ESCS.

Cases are 2 Japanese patients who were reported previously.[3] Case 1 was a 31-year-old man whose parents were consanguineous. His vision was 0.7 in the right eye and 0.3 in the left eye. Funduscopy revealed retinal degeneration surrounding the vascular arcade with cystic changes in both maculae (Fig 2, available online at http://aaojournal.org). Perimetry showed ring-shaped scotoma and electrophysiology showed unique responses corresponding to ESCS (Figs 3–6, available online at http://aaojournal.org). During 23-year clinical follow-up, clumped pigmentation has appeared in the retinal degeneration and the cystic changes in the foveal region have become ambiguous (Fig 2). His latest vision was 0.5 in the right eye and 0.3 in the left eye at age 53.

Genetic analysis revealed a novel nucleotide substitution (c.151G>A) in exon 2 homozygously, resulting in a novel missense mutation (a glycine-to-arginine substitution) at amino acid position 51 (p.G51R; Fig 7; available online at http://aaojournal.org).

Case 2 was a 78-year-old woman.[3] Funduscopy showed diffuse mild retinal degeneration with no pigmentation in both eyes (Fig 8, available online at http://aaojournal.org). Optical coherence tomography showed a subtle foveal schisis in the left eye, although the structure of the retina including the outer nuclear layer in the macular area was relatively well maintained (Fig 8). After cataract surgery, her vision improved to 0.3 in the right eye and 0.2 in the left.

Genetic analysis revealed compound heterozygous mutations of c.142C>T (exon 2) and c.311G>A (exon 3), resulting in an arginine-to-cysteine substitution at amino acid position 48 (p.R48C) and an arginine-to-glutamine substitution at amino acid position 104 (p.R104Q; Fig 7).

A daughter of case 2 who was asymptomatic and had normal fundus appearance showed only the p.R48C mutation heterozygously, that indicated she was an unaffected carrier relative (Fig 7).

NR2E3 protein, a photoreceptor-specific orphan nuclear receptor, plays an important role in the development and differentiation of rods and all cone classes. NR2E3 has 2 functionally important domains, namely, the DNA-binding domain (DBD) and the ligand-binding domain (Fig 1). Mutations within these domains result in serious dysfunction of NR2E3 protein leading to abnormal process of development and differentiation of multipotent progenitor cells to rods and cones.

Genetic analysis revealed a homozygous mutation (p.G51R) in case 1 and compound heterozygous mutations of (p.R48C) and (p.R104Q) in case 2. Among these mutations, (p.G51R) and (p.R48C) are novel as causative mutations of ESCS.

The mutation (p.G51R) found in case 1 resides in the first zinc finger of the DBD, and the compound heterozygous mutations (p.R48C and p.R104Q), which were found in case 2 reside in the first and second zinc fingers of the DBD. Because the zinc fingers are necessary for maintenance the structure of NR2E3 protein, these mutations in the zinc fingers of NR2E3 result in phenotypes as ESCS (Fig 1).

Clinically, case 1 with a homozygous missense mutation (p.G51R) showed typical features as ESCS, whereas case 2 with compound heterozygous mutations (p.R48C and p.R104Q) showed mild retinal degeneration and has kept some level of vision and construction of the macula despite advanced age. In the past, the mutation (p.R104Q) has never been reported except in 1 case, which demonstrated the normal structure and function of the macula with recordable rod electrophysiology.[5] These facts indicate the mutation (p.R104Q) may be correlated with the relatively mild clinical findings as ESCS.

We identified 2 novel missense mutations (p.G51R and p.R48C) as causes of ESCS. To our knowledge, the finding of case 1 is the longest-observed clinical case ever reported, and case 2 is the oldest case among all the patients with ESCS so far reported.

Kazuki Kuniyoshi, MD,[1] Takaaki Hayashi, MD,[2] Hiroyuki Sakuramoto, MD,[1] Akira Nakao, MD,[1]
Takashi Sato, MD,[1] Tomohiro Utsumi,[2] Hiroshi Tsuneoka, MD,[2] Yoshikazu Shimomura, MD[1]

[1]Department of Ophthalmology, Kinki University, Faculty of Medicine, Osaka, Japan; [2]Department of Ophthalmology, The Jikei University School of Medicine, Tokyo, Japan

References

1. Marmor MF, Jacobson SG, Foerster MH, et al. Diagnostic clinical findings of a new syndrome with night blindness, maculopathy, and enhanced S cone sensitivity. Am J Ophthalmol 1990;110:124–34.
2. Jacobson SG, Marmor MF, Kemp CM, Knighton RW. SWS (blue) cone hypersensitivity in a newly identified retinal degeneration. Invest Ophthalmol Vis Sci 1990;31:827–38.
3. Sato T, Kuniyoshi K, Nakao A, et al. Long-term observation of two cases of enhanced S-cone syndrome. J Jpn Ophthalmol Soc 2009;113:980–90.
4. Haider NB, Jacobson SG, Cideciyan AV, et al. Mutation of a nuclear receptor gene, *NR2E3*, causes enhanced S cone syndrome, a disorder of retinal cell fate. Nat Genet 2000;24:127–31.
5. Hayashi T, Gekka T, Goto-Omoto S, et al. Novel *NR2E3* mutations (R104Q, R334G) associated with a mild form of enhanced S-cone syndrome demonstrate compound heterozygosity. Ophthalmology 2005;112:2115–22.

Financial Support: This study was supported by grants from the Ministry of Health, Labour and Welfare of Japan and the Vehicle Racing Commemorative Foundation.

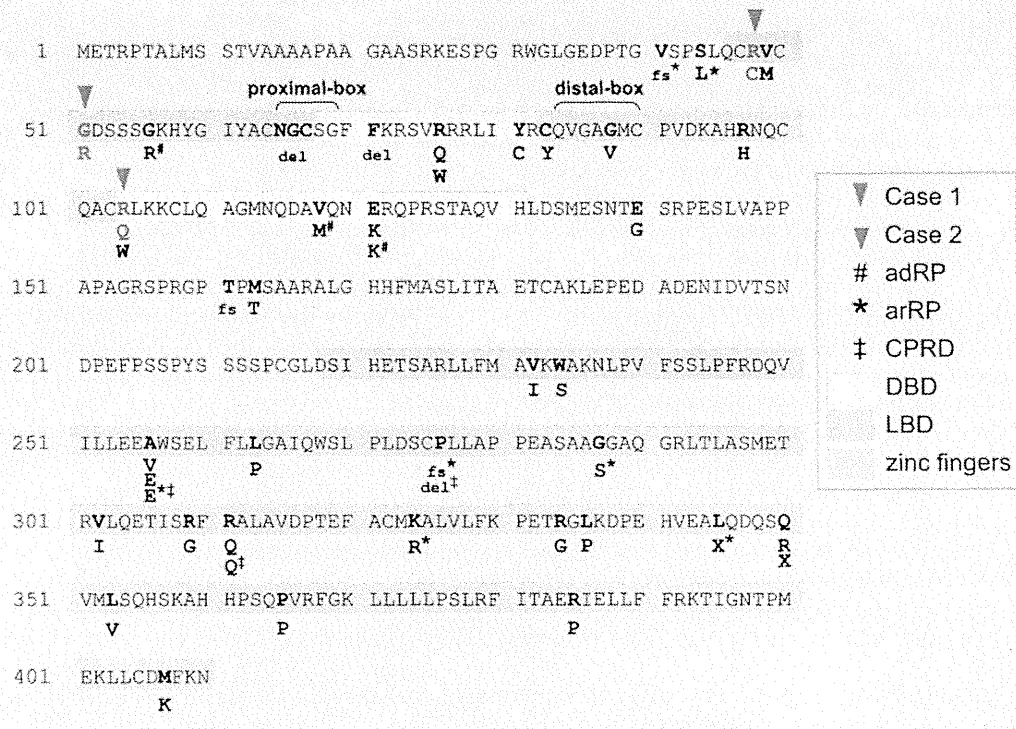

Figure 1. NR2E3 protein structure and mutations in cases presented in this letter and reported in past papers. Bold characters with no marks indicate mutations reported as a cause of enhanced S-cone syndrome (ESCS). Red characters and arrow indicate homozygous missense mutation discovered in Case 1 (p.G51R). Blue characters and arrows indicate compound heterozygous missense mutations discovered in case 2 (p.R48C and p.R104Q). p.G51R and p.R48C are novel mutations as causes of ESCS. adRP = autosomal-dominant retinitis pigmentosa; arRP = autosomal-recessive retinitis pigmentosa; CPRD = clumped pigmentary retinal degeneration; DBD = DNA-binding domain; del = deletion mutation; fs = frame shift of amino acids; LBD = ligand-binding domain.

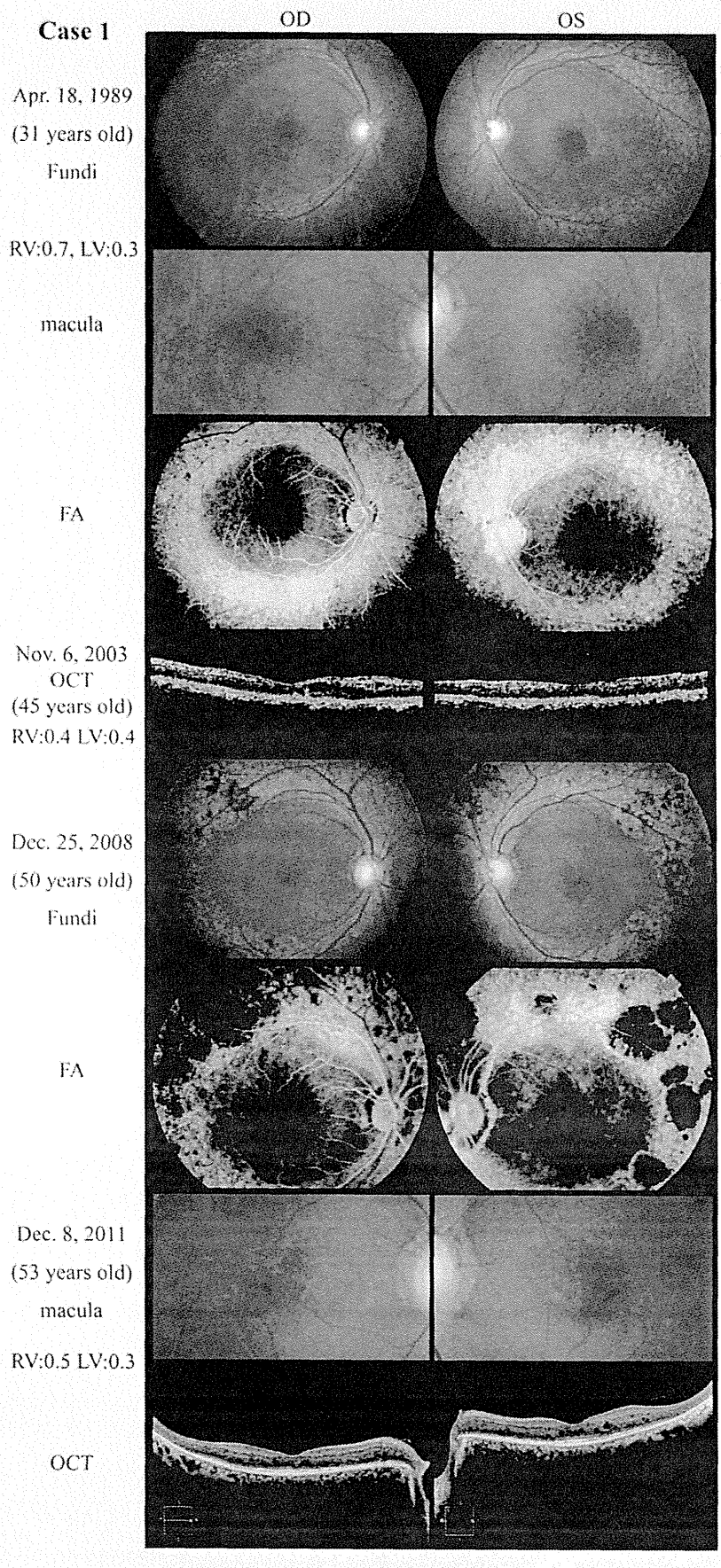
Case 1
OD
OS
Apr. 18, 1989
(31 years old)
Fundi
RV:0.7, LV:0.3
macula
FA
Nov. 6, 2003
OCT
(45 years old)
RV:0.4 LV:0.4
Dec. 25, 2008
(50 years old)
Fundi
FA
Dec. 8, 2011
(53 years old)
macula
RV:0.5 LV:0.3
OCT